

Chirped fractional stimulated Raman adiabatic passage

Jabir Chathanathil ^{1,2}, Aneesh Ramaswamy,¹ Vladimir S. Malinovsky ²,
Dmitry Budker ^{3,4} and Svetlana A. Malinovskaya ^{1,3,5}

¹*Department of Physics, Stevens Institute of Technology, Hoboken, New Jersey 07030, USA*

²*DEVCOM Army Research Laboratory, Adelphi, Maryland 20783, USA*

³*Helmholtz-Institut Mainz, Johannes Gutenberg-Universität Mainz, 55128 Mainz, Germany*

⁴*Department of Physics, University of California, Berkeley, Berkeley, California 94720, USA*

⁵*Institut für Angewandte Physik, Technische Universität Darmstadt, 64289 Darmstadt, Germany*



(Received 14 July 2023; accepted 25 September 2023; published 13 October 2023)

In this work we develop a theory of fractional stimulated Raman adiabatic passage (FSTIRAP) using frequency-chirped pulses (CFSTIRAP). We analyze the CFSTIRAP as a method to create a coherent superposition state maximizing coherence between the initial and the target state in the presence of the two-photon detuning. We demonstrate that the pulse chirping permits relaxation of the condition of the two-photon resonance required for adiabatic passage in STIRAP and FSTIRAP. The choice of the chirp rate $|\alpha| = |\delta|/(t_p - t_s)$ enables adiabatic passage to a predetermined state between two nearly degenerate final states within a broad range of values of the two-photon detuning and the chirp rate. The proposed schemes will expand the scope of quantum control methods and contribute to the further improvement of quantum imaging, sensing, and metrology.

DOI: [10.1103/PhysRevA.108.043710](https://doi.org/10.1103/PhysRevA.108.043710)

I. INTRODUCTION

Since its discovery, stimulated Raman adiabatic passage (STIRAP) has developed into a prominent method of quantum coherent control [1]. Owing to its robustness, STIRAP has been used in a variety of research fields, as detailed in the road-map provided in [2]. The applications of STIRAP continue to expand, advancing state control in solid-state materials, e.g., nitrogen-vacancy (NV) centers [3] and silicon-vacancy centers in the diamond [4], creating ultracold molecules using mixed intermediate states [5], performing geometric gates in superconducting qubits by implementing shortcuts to adiabaticity [6,7], mastering nuclear coherent population transfer to the $^{229\text{m}}\text{Th}$ isomer using x-ray pulses [8], efficiently swapping population from an arbitrary initial state [9], designing a digitized version of STIRAP [10], and imaging stars via quantum communication techniques [11].

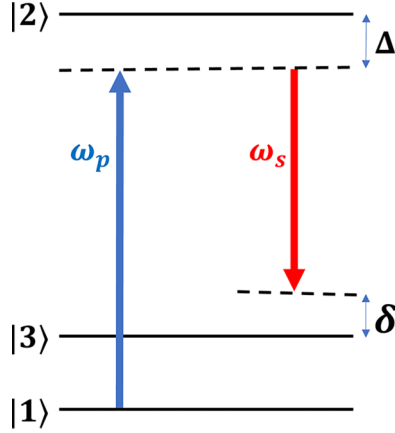
An extension of STIRAP, the fractional STIRAP (FSTIRAP), may prove useful for imaging, sensing and detection by virtue of the generation of an enhanced signal as well as the signal sustainability upon propagation through a medium. Fractional STIRAP is designed to generate a coherent superposition of the initial and the final states by manipulating the duration of the Stokes pulse and make it vanishing simultaneously with the pump pulse [12]. For example, FSTIRAP was applied in experiments in Rb atomic vapor to maximize atomic coherence, which led to the enhancement of coherent Raman scattering [13]. The practicality of this method is based on a relative flexibility of the key control parameters relevant for both STIRAP and FSTIRAP such as the fields strength, the ratio of the pump to the Stokes Rabi frequency, the Stokes pump pulse delay, and the pulse duration. The implementation of ultrafast chirped pulses brings spectroscopic advantages, as shown in a number of papers [14–17]. In [18], STIRAP with chirped pulses permitted the selective excitation

of two nearly degenerate states by changing the sign of the chirp. However, FSTIRAP has never been examined for the degree of spectral resolution for imaging and detection techniques. This motivated us to explore thoroughly the effects of chirping pulses in STIRAP as well as FSTIRAP processes. We show that chirping both pulses with equal rates in CSTIRAP cancels out the nonadiabatic term caused by the two-photon detuning and thus preserves adiabatic passage within the dark state. Moreover, in a system with two nearly degenerate final states, the population can be driven to a desired state by controlling the sign of the chirp of the Stokes and the pump pulses. In CFSTIRAP, chirping of the pulses results in an improved selectivity in the creation of the maximum coherence between the initial and a predetermined final state. Another technique, the chirped adiabatic passage (CHIRAP), has been used for selective population transfer to one of the fine-structure states in Na vapor [19,20]. It differs from CSTIRAP in that CHIRAP does not have a time delay between pulses.

The paper is organized as follows. After a brief discussion of conventional STIRAP and FSTIRAP, we examine in detail the configuration of CSTIRAP and explain the selective excitation of nearly degenerate final states through the dressed-state analysis. Next we address the CFSTIRAP and show how the control scheme of the selective excitation is modified for the formation of a final coherent superposition state.

II. STIRAP AND FSTIRAP

In conventional STIRAP, the pump and the Stokes pulses interact with a three-level system, making a complete adiabatic population transfer from the initial state to the final state. The schematic diagram of the three-level λ system in application to STIRAP is shown in Fig. 1, where $\omega_{p,s}$ represent the


 FIG. 1. Coupling scheme of STIRAP in the three-level λ system.

carrier frequencies of the pump and the Stokes fields, respectively. The one-photon and the two-photon detunings are $\Delta = \omega_2 - \omega_1 - \omega_p$ and $\delta = \omega_p - \omega_s - (\omega_3 - \omega_1)$, respectively.

The Hamiltonian describing the interaction of the three-level system with the pump $E_p(t)$ and the Stokes $E_s(t)$ pulses is

$$\mathbf{H}(t) = \sum_{i=1}^3 \hbar\omega_i |i\rangle\langle i| - [\mu_{21}E_p(t)|1\rangle\langle 2| + \text{H.c.}] - [\mu_{23}E_s(t)|3\rangle\langle 2| + \text{H.c.}] \quad (1)$$

The dynamics of the system is governed by the Schrödinger equation

$$i\hbar \frac{\partial}{\partial t} |\psi(t)\rangle = \mathbf{H}(t) |\psi(t)\rangle, \quad |\psi(t)\rangle = \sum_{n=1}^3 a_n(t) |n\rangle. \quad (2)$$

In STIRAP, the $E_{p,s}(t)$ are the Gaussian fields with carrier frequencies $\omega_{p,s}$ and central times $t_{p,s}$,

$$E_{p,s}(t) = E_{p_0,s_0} e^{-(t-t_{p,s})^2/\tau_{p,s}^2} \cos[\omega_{p,s}(t-t_{p,s})]. \quad (3)$$

The counterintuitive sequence of pulses and suitable overlap between the Gaussian envelopes, which is determined by the delay $t_p - t_s$, is necessary to perform the adiabatic evolution of population from $|1\rangle$ to $|3\rangle$ [21].

While STIRAP is used for full population transfer, the scheme of FSTIRAP is intended to partially preserve the population in the ground state, thus creating a coherent superposition of the initial and the final states by the end of the pulse sequence. The approach implies elongating the Stokes pulse so that it vanishes simultaneously with the pump pulse. For this reason, the pump and the Stokes fields are modified as

$$E_p(t) = E_{p_0} \sin A e^{-(t-t_p)^2/\tau^2} \cos[\omega_p(t-t_p)], \\ E_s(t) = E_{s_0} e^{-(t+t_p)^2/\tau^2} \cos[\omega_s(t+t_p)] \\ + E_{s_0} \cos A e^{-(t-t_p)^2/\tau^2} \cos[\omega_s(t-t_p)], \quad (4)$$

where the Stokes field is composed of two Stokes pulses having central times t_p and $-t_p$. Note that, for $A = \pi/2$, substituting $t_p = -t_s$ in the Stokes field equation provides the fields in Eq. (3) relevant for STIRAP. Substituting Eq. (4) in

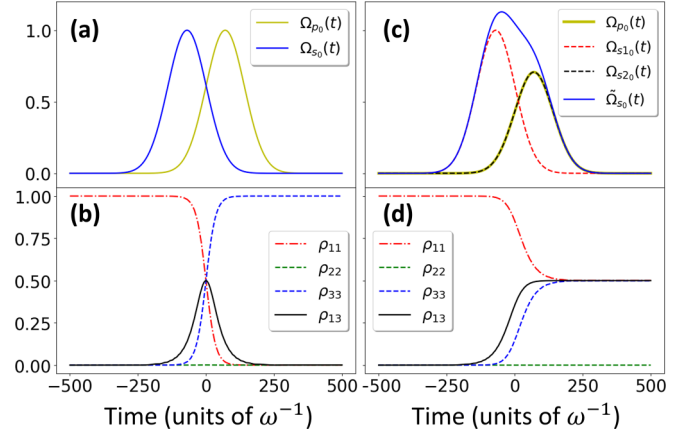


FIG. 2. Pump and Stokes Rabi frequencies and population dynamics in STIRAP and FSTIRAP. In STIRAP, (a) the Gaussian Rabi frequency of the pump and the Stokes pulses are shown with a delay between them, resulting in (b) a full population transfer from the initial state to the final state. (c) In FSTIRAP, the Stokes Rabi frequency (represented by the blue solid curve) consists of two Gaussian components Ω_{s1_0} and Ω_{s2_0} . Note that $\Omega_{p_0}(t)$ overlaps exactly with the second Stokes component $\Omega_{s2_0}(t)$. (d) With this sequence of pulses, coherence ρ_{13} is maximized.

(1), applying the transformations

$$a_1(t) = \tilde{a}_1(t) e^{i\omega_p(t-t_p)}, \\ a_2(t) = \tilde{a}_2(t), \\ a_3(t) = \tilde{a}_3(t) e^{i\omega_s(t+t_p)} \quad (5)$$

in the Schrödinger equation (2), and using the rotating-wave approximation gives the field-interaction Hamiltonian of the three-level system describing FSTIRAP,

$$\mathbf{H}(t) = \frac{\hbar}{2} \begin{pmatrix} 0 & \Omega_{p_0}(t) & 0 \\ \Omega_{p_0}(t) & 2\Delta & \Omega_{s1_0}(t) + \Omega_{s2_0}(t) e^{i\zeta} \\ 0 & \Omega_{s1_0}(t) + \Omega_{s2_0}(t) e^{-i\zeta} & -2\delta \end{pmatrix}, \quad (6)$$

where the Rabi frequencies are

$$\Omega_{p_0}(t) = \Omega_0 \sin A e^{-(t-t_p)^2/\tau^2}, \\ \Omega_{s1_0}(t) = \Omega_0 e^{-(t+t_p)^2/\tau^2}, \\ \Omega_{s2_0}(t) = \Omega_0 \cos A e^{-(t-t_p)^2/\tau^2}, \quad (7)$$

with $\Omega_0 = -E_{p_0}\mu_{21}/\hbar = -E_{s_0}\mu_{32}/\hbar$ and the phase given by $\zeta = 2\omega_s t_p$. With an appropriate choice of t_p satisfying the condition such that $2\omega_s t_p = 2n\pi$, with n an integer and $t_p = n\pi/\omega_s$, the phase dependence is canceled out, e.g., for $t_p = 71$, $\omega_s = 5$, and $e^{-i\zeta} \approx 1$. Note again that the conventional STIRAP Hamiltonian can be retrieved from Eq. (6) by taking $A = \pi/2$ and substituting $t_p = -t_s$ in the Stokes Rabi frequency.

The pulse sequence and the time evolution of populations in STIRAP as well as FSTIRAP are given in Fig. 2. The pump and Stokes Rabi frequencies of the Gaussian shape [Fig. 2(a)] transfer the population from $|1\rangle$ to $|3\rangle$ [Fig. 2(b)]. The parameter that distinguishes the dynamics of STIRAP

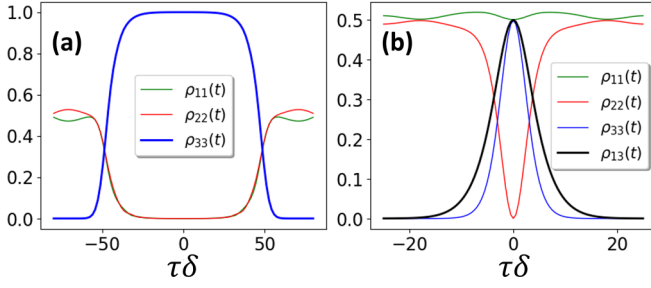


FIG. 3. State populations and coherence in (a) STIRAP and (b) FSTIRAP as a function of $\tau\delta$. In STIRAP, the population is fully transferred to the final state in the vicinity of the two-photon resonance $\delta = 0$. Here $\Omega_0 = 1.0\omega$ and $\tau = 100\omega^{-1}$.

and FSTIRAP is the mixing angle $\theta(t)$, which is given by $\theta(t) = \tan^{-1}[\Omega_{p_0}(t)/\Omega_{s_0}(t)]$. For STIRAP $\theta(t \rightarrow -\infty) = 0$ and $\theta(t \rightarrow \infty) = \pi/2$, while for FSTIRAP $\theta(t \rightarrow -\infty) = 0$ and $\theta(t \rightarrow \infty) = A$, where $\pi/4 \geq A \geq \pi/2$. By varying the constant mixing angle A , any arbitrary superposition state having coherence up to its maximum value $1/2$ can be created. For $A = \pi/4$, the $\Omega_{p_0}(t)$ perfectly overlaps with the second component of the Stokes Rabi frequency $\Omega_{s_2_0}(t)$, and they vanish simultaneously as shown in Fig. 2(c), maximizing coherence ρ_{13} , shown in Fig. 2(d).

Conceptually, the two-photon resonance is required for adiabatic passage to occur within the dark state in STIRAP [22]. The end-of-STIRAP state populations are depicted in Fig. 3(a) as a function of $\tau\delta$. A complete population transfer to the final state is observed in the vicinity of the two-photon resonance. However, for nonzero values of δ , the evolution of populations is not adiabatic, as it will be demonstrated in the next section, and the transfer to the final state is compromised by the admixture of the transitional state. Analogous to the case of STIRAP, the two-photon resonance is required to maximize coherence in FSTIRAP. We investigate how coherence reduces from the maximum value with the increase of the two-photon detuning in FSTIRAP, which is shown in Fig. 3(b). The reduction of coherence from the maximum value by the factor of 2 is observed for $\tau\delta = 5$.

III. CSTIRAP

A. CSTIRAP in a three-level λ system

Here we demonstrate that the two-photon resonance condition for adiabatic passage within the dark state can be bypassed by chirping the input pulses in STIRAP. Consider the pump and the Stokes pulses chirped with the rates $\alpha_{p,s}$,

respectively,

$$E_{p,s}(t) = E_{p_0,s_0} e^{-(t-t_{p,s})^2/\tau_{p,s}^2} \cos \left(\omega_{p,s}(t-t_{p,s}) + \frac{\alpha_{p,s}}{2}(t-t_{p,s})^2 \right). \quad (8)$$

To derive the field-interaction Hamiltonian for CSTIRAP, we apply the following transformations to the probability amplitudes in Eq. (2):

$$\begin{aligned} a_1(t) &= \tilde{a}_1(t) e^{i\omega_p(t-t_p) + (i/2)\alpha_p(t-t_p)^2}, \\ a_2(t) &= \tilde{a}_2(t), \\ a_3(t) &= \tilde{a}_3(t) e^{i\omega_s(t-t_s) + (i/2)\alpha_s(t-t_s)^2}. \end{aligned} \quad (9)$$

Then, under the rotation-wave approximation, the Hamiltonian reads

$$\mathbf{H}(t) = \frac{\hbar}{2} \begin{pmatrix} 0 & \Omega_{p_0}(t) & 0 \\ \Omega_{p_0}(t) & 2\Delta(t) & \Omega_{s_0}(t) \\ 0 & \Omega_{s_0}(t) & 2\delta(t) \end{pmatrix}, \quad (10)$$

where the time-dependent one-photon and two-photon detunings are defined as $\Delta(t) = \Delta - \alpha_p(t-t_p)$ and $\delta(t) = -\delta + \alpha_s(t-t_s) - \alpha_p(t-t_p)$, respectively. A closer look at the dressed-state picture in CSTIRAP shows that with the right choice of chirp rates, an adiabatic transition is possible even at $\delta \neq 0$.

B. Dressed-state analysis of CSTIRAP: A three-level λ system

Consider a unitary rotation matrix $\mathbf{T}(t)$,

$$\mathbf{T}(t) = \begin{pmatrix} \sin \theta(t) \sin \phi(t) & \cos \theta(t) & \sin \theta(t) \cos \phi(t) \\ \cos \phi(t) & 0 & -\sin \phi(t) \\ \cos \theta(t) \sin \phi(t) & -\sin \theta(t) & \cos \theta(t) \cos \phi(t) \end{pmatrix}, \quad (11)$$

with mixing angles

$$\begin{aligned} \tan \theta(t) &= \frac{\Omega_{p_0}(t)}{\Omega_{s_0}(t)}, \\ \tan 2\phi(t) &= \frac{\sqrt{|\Omega_{p_0}(t)|^2 + |\Omega_{s_0}(t)|^2}}{\Delta(t)}. \end{aligned} \quad (12)$$

Rotation of the probability amplitudes $\tilde{\mathbf{a}}(t)$ using matrix $\mathbf{T}(t)$ gives the dressed-state probability amplitudes $\mathbf{c}_d(t) = \mathbf{T}^\dagger(t)\tilde{\mathbf{a}}(t)$; in the dressed-state basis the Hamiltonian $\mathbf{H}_d(t)$ reads

$$\begin{aligned} \mathbf{H}_d(t) &= \mathbf{T}^\dagger(t)\mathbf{H}(t)\mathbf{T}(t) - i\hbar\mathbf{T}^\dagger(t)\dot{\mathbf{T}}(t) \\ &= \hbar \begin{pmatrix} \lambda_+(t) & 0 & 0 \\ 0 & \lambda_0(t) & 0 \\ 0 & 0 & \lambda_-(t) \end{pmatrix} + \hbar\delta(t)\cos^2\theta(t) \begin{pmatrix} \sin^2\phi(t) & -\tan\theta(t)\sin\phi(t) & \frac{1}{2}\sin 2\phi(t) \\ -\tan\theta(t)\sin\phi(t) & \tan^2\theta(t) & -\tan\theta(t)\sin\phi(t) \\ \frac{1}{2}\sin 2\phi(t) & -\tan\theta(t)\sin\phi(t) & \cos^2\phi(t) \end{pmatrix} \\ &\quad - i\hbar \begin{pmatrix} 0 & -\dot{\theta}(t)\sin\phi(t) & -\dot{\phi}(t) \\ \dot{\theta}(t)\sin\phi(t) & 0 & \dot{\theta}(t)\cos\phi(t) \\ \dot{\phi}(t) & -\dot{\theta}(t)\cos\phi(t) & 0 \end{pmatrix}, \end{aligned} \quad (13)$$

where

$$\begin{aligned}\lambda_+(t) &= \frac{1}{2} \left\{ \Delta(t) + \sqrt{[\Delta(t)]^2 + |\Omega_{p_0}(t)|^2 + |\Omega_{s_0}(t)|^2} \right\}, \\ \lambda_0(t) &= 0, \\ \lambda_-(t) &= \frac{1}{2} \left\{ \Delta(t) - \sqrt{[\Delta(t)]^2 + |\Omega_{p_0}(t)|^2 + |\Omega_{s_0}(t)|^2} \right\}.\end{aligned}\quad (14)$$

For the process to be adiabatic, the dressed-state Hamiltonian $\mathbf{H}_d(t)$ needs to be diagonal. The nonadiabatic contribution due to the second term in Eq. (13) is canceled out by imposing the time-dependent two-photon detuning $\delta(t) = -\delta + \alpha_s(t - t_s) - \alpha_p(t - t_p)$ to be zero. This can be done by choosing the chirp rates such that $-\delta + (\beta - \alpha)t + \alpha t_p - \beta t_s = 0$, where $\alpha = \alpha_p$ and $\beta = \alpha_s$. If α and β are chosen to be equal, this condition becomes $\alpha(t_p - t_s) = \delta$ and the choice of t_p , t_s , and α satisfying this condition eliminates the $\delta(t)$ -dependent nonadiabatic term.

The third term in Eq. (13) constitutes the nonadiabatic contribution from $\mathbf{T}^\dagger(t)\mathbf{T}(t)$, with $\dot{\theta}(t)$ and $\dot{\phi}(t)$ given by

$$\begin{aligned}\dot{\theta}(t) &= \frac{\Omega_{s_0}\dot{\Omega}_{p_0} - \Omega_{p_0}\dot{\Omega}_{s_0}}{\Omega_{p_0}^2 + \Omega_{s_0}^2}, \\ \dot{\phi}(t) &= \frac{\Delta(\Omega_{p_0}\dot{\Omega}_{p_0} + \Omega_{s_0}\dot{\Omega}_{s_0}) - \dot{\Delta}(\Omega_{p_0}^2 + \Omega_{s_0}^2)}{2\sqrt{\Omega_{p_0}^2 + \Omega_{s_0}^2}(\Delta^2 + \Omega_{p_0}^2 + \Omega_{s_0}^2)}.\end{aligned}\quad (15)$$

For adiabatic passage, the contribution from the third term must be negligible, requiring $|\dot{\theta}(t)|, |\dot{\phi}(t)| \ll |\lambda_{\pm}(t)|$. The conditions for mixing angles $\theta(t)$ and $\phi(t)$ are met in the presence of a significant overlap between the Stokes and the pump pulses with $\theta(t)$ and $\phi(t)$ varying very slowly.

When these adiabaticity conditions are satisfied, the dressed state having the zero energy $\lambda_0(t) = 0$ is given by

$$|\lambda_0(t)\rangle = \cos\theta(t)|\tilde{1}\rangle - \sin\theta(t)|\tilde{3}\rangle. \quad (17)$$

This state, known as the dark state, smoothly evolves from the initial bare state $|\tilde{1}\rangle$ to the final bare state $|\tilde{3}\rangle$ without having any component of the intermediate state $|\tilde{2}\rangle$. For the remainder of this section, the tilde of the wave function and eigenstates is dropped for convenience. The frequency and time parameters in this paper are expressed in the units of ω and ω^{-1} respectively where ω is an arbitrary frequency.

Adiabatic population transfer in the presence of nonzero two-photon detuning is demonstrated in Fig. 4. Here the evolution of the dressed-state energies $\lambda_{0,\pm}$, the nonadiabatic coupling parameter $V_{0,\pm}$, the state populations, and coherence are given for the chirp rates satisfying the condition $\delta(t) = 0$. In Figs. 4(a) and 4(b), δ and α are positive, and in Figs. 4(c) and 4(d), these parameters are negative. In both cases, the two-photon detuning δ is compensated by $\alpha(t_p - t_s)$ and the system dynamics is always aligned with the dark state having energy $\lambda_0(t) = 0$; the population is completely transferred adiabatically from the initial bare state $|1\rangle$ to the final bare state $|3\rangle$ without populating the intermediate state $|2\rangle$. Intuitively, this process can be explained in the following way: Since both the pump and the Stokes fields are chirped at the same rate, both their frequencies sweep through the energy levels at the same rate. However, because of the delay $t_p - t_s$ between the two pulses, a factor of $\alpha(t_p - t_s)$ needs to be

added to the detuning to keep the system in resonance during the process.

The robustness of this population is demonstrated in Fig. 5, where the final-state population ρ_{33} is plotted as a function of the two-photon detuning δ and the chirp rate α . A broad area in the vicinity of the dark line satisfying the condition $\alpha = \delta/(t_p - t_s)$ indicates the robustness of this scheme. It should be noted that the robustness around $\delta = 0$ in STIRAP is symmetric, as is evident from Fig. 3(a), while for a given δ it is not symmetric around $\delta = \alpha(t_p - t_s)$ in CSTIRAP.

C. CSTIRAP in a four-level λ system with two energetically close final states

Consider a system with an additional level nearly degenerate with the final state in the λ configuration. A schematic of such a system is shown in Fig. 6 with the two-photon resonance occurring with state $|3\rangle$, which implies the two-photon detuning is $\delta' = \omega_p - \omega_s - (\omega_4 - \omega_1)$ and the one-photon detuning is $\Delta = \omega_2 - \omega_1 - \omega_p$. In the rotating-wave approximation and the field-interaction representation, the Hamiltonian of the four-level system is

$$H(t) = \frac{\hbar}{2} \begin{pmatrix} 0 & \Omega_{p_0}(t) & 0 & 0 \\ \Omega_{p_0}(t) & 2\Delta(t) & \Omega_{s_0}(t) & \Omega_{s_0}(t) \\ 0 & \Omega_{s_0}(t) & 2[\delta'(t) + \delta'] & 0 \\ 0 & \Omega_{s_0}(t) & 0 & 2\delta'(t) \end{pmatrix}, \quad (18)$$

where $\Delta(t)$ and $\delta'(t)$ are defined as $\Delta(t) = \Delta - \alpha(t - t_p)$ and $\delta'(t) = -\delta' + \beta(t - t_s) - \alpha(t - t_p)$. With the choice of equal chirp rates for the pump and the Stokes pulses, $\beta = \alpha$, the fourth diagonal term in the Hamiltonian can be canceled out by fulfilling the condition $\alpha = \delta'/(t_p - t_s)$. This is a sufficient condition for transferring the population to the

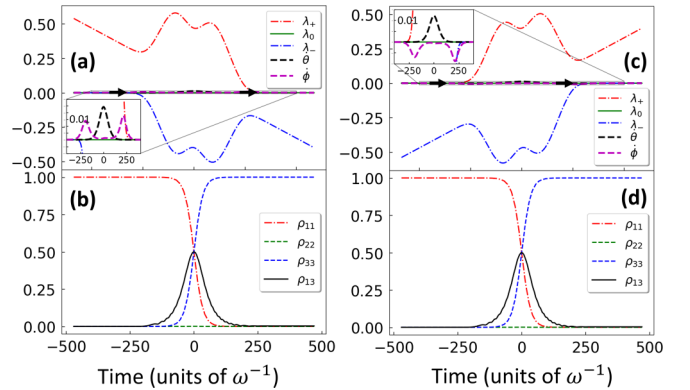


FIG. 4. Evolution of the dressed-state energies and populations in the CSTIRAP when (a) and (b) $\delta > 0$ and (c) and (d) $\delta < 0$. The population is adiabatically transferred from the initial state to the final state in both cases, owing to the choice of the chirp rates satisfying $\delta(t) = -\delta + \alpha(t_p - t_s) = 0$, where $\alpha = \beta$. The nonadiabatic coupling parameters $\dot{\theta}$ and $\dot{\phi}$ are very small compared to $|\lambda_+ - \lambda_-|$ during the interaction, as shown in the inset, implying the adiabatic nature of interaction. Here (a) and (b) $\delta = 0.14\omega$ and $\alpha = 1 \times 10^{-3}\omega^2$ and (c) and (d) $\delta = -0.14\omega$ and $\alpha = -1 \times 10^{-3}\omega^2$. The other parameters are $\Delta = 0$, $t_s = -70\omega^{-1}$, $t_p = 70\omega^{-1}$, $\tau_{p,s} = 100\omega^{-1}$, and peak Rabi frequencies $\Omega_{p_0,s_0} = 1.0\omega$.

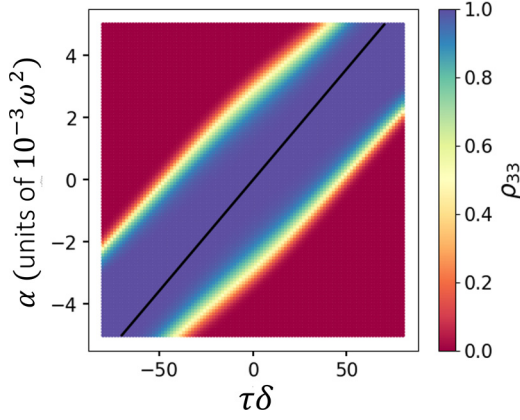


FIG. 5. Final-state population in CSTIRAP as a function of the two-photon detuning and the chirp rate. The adiabatic population transfer is achieved in the vicinity of the dark line satisfying $\alpha = \delta/(t_p - t_s)$, providing $\delta(t) = 0$.

detuned state $|4\rangle$ adiabatically. This condition implies that both the chirp rate and the two-photon detuning δ' need to be of the same sign. In contrast, choosing the chirp rate equal to $\alpha = -\delta'/(t_p - t_s)$ results in transferring population to the resonant state $|3\rangle$; in this case, the signs of the detuning and the chirp are opposite. In numerical analysis, the values of the peak Rabi frequency and the time duration are taken to be $\Omega_{p,s_0} = 1.0\omega$ and $\tau_{p,s} = 100\omega^{-1}$. The dynamics of the selective population transfer to each of the final states is shown in Fig. 7. In Fig. 7(a) the bare state $|4\rangle$ is populated at the end of pulse sequence with the choice of $\alpha = 1 \times 10^{-3}\omega^2$, and in Fig. 7(b) the population is driven to the final bare state $|3\rangle$ with the choice of the negative chirp $\alpha = -1 \times 10^{-3}\omega^2$.

Figure 8 shows the contour plots of populations of states $|4\rangle$ [Fig. 8(a)] and $|3\rangle$ [Fig. 8(b)] as a function of detuning δ' and chirp rate α . The dark solid line in Fig. 8(a) represents the constraint condition $-\delta' + \alpha(t_p - t_s) = 0$. For selective excitation of state $|4\rangle$, the chirp and the detuning must be chosen in the vicinity of this line, implying that both of them have the same sign. The condition to drive the transition to

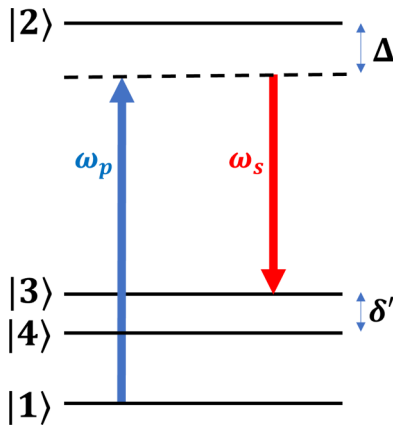


FIG. 6. Four-level λ system of the STIRAP configuration having two energetically close final states. The two-photon resonance is with state $|3\rangle$ and the two-photon detuning from state $|4\rangle$ is $\delta' = \omega_p - \omega_s - (\omega_4 - \omega_1)$; the one-photon detuning is $\Delta = \omega_2 - \omega_1 - \omega_p$.

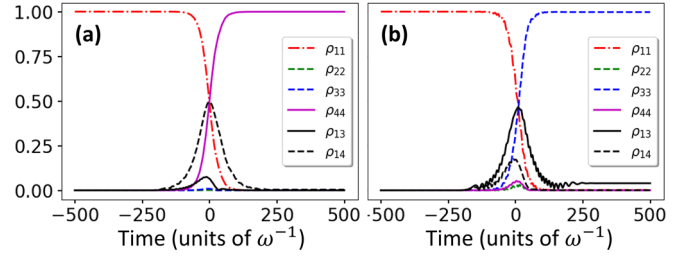


FIG. 7. Selective population transfer in the four-level STIRAP scheme achieved by controlling the sign of the chirp rate in the case of positive two-photon detuning $\delta' = 0.14\omega$. (a) The detuned state $|4\rangle$ is populated owing to a positive chirp rate given by $\alpha = \delta'/(t_p - t_s)$, where $\alpha = \beta$. (b) In contrast, the population is transferred to the resonant state $|3\rangle$ with a negative chirp rate given by $\alpha = -\delta'/(t_p - t_s)$. The parameters are $\Delta = 0$, $t_s = -70\omega^{-1}$, $t_p = 70\omega^{-1}$, $\tau_{p,s} = 100\omega^{-1}$, and the peak Rabi frequencies $\Omega_{p,s_0} = 1.0\omega$. The values of the chirp rates are $\alpha = \pm 1 \times 10^{-3}\omega^2$.

state $|3\rangle$ is $\delta' + \alpha(t_p - t_s) = 0$ [represented by the dark dashed line in Fig. 8(b)], implying that the signs of the detuning and the chirp need to be opposite. For zero detuning, states $|3\rangle$ and $|4\rangle$ are degenerate and are equally populated. When detuning deviates from zero, the detuned state is selectively populated if the chirp has the same sign as the detuning or the population goes solely to the resonant state if the signs of the chirp and the detuning are opposite. The latter case implies that the nonadiabatic term is not canceled out however, meaning the nonadiabatic term proportional to $\delta(t)$ is not zero. The dressed-state analysis indeed demonstrates that the evolution of the wave function in this case involves a series of dressed states. Surprisingly enough, even under the condition of nonadiabatic coupling between dressed states, the range of α and δ' parameters is broad and demonstrates the robustness of the approach. Such a dependence of the state dynamics on the sign of detuning and the chirp is further explained in the next section by analyzing the evolution of the dressed states in the field-interaction frame.

D. Dressed-state analysis of CSTIRAP in the four-level λ system

If in the three-level CSTIRAP the transformation to a dressed-state basis can be done using a three-dimensional rotation matrix, it is not so trivial in the case of the four-level

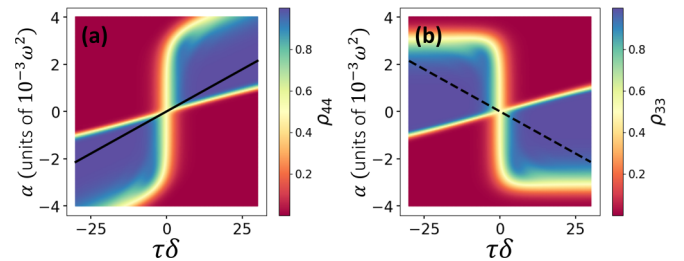


FIG. 8. Populations of states (a) $|4\rangle$ and (b) $|3\rangle$ as a function of δ' and α . The dark solid line represents the constraint condition $\delta'(t) = 0$ and $\delta'/(t_p - t_s) = \alpha$ for the selective excitation of state $|4\rangle$. For state $|3\rangle$ selective excitation, the constraint condition is $-\delta'/(t_p - t_s) = \alpha$, which does not cancel out $\delta'(t)$ and that is the cause of nonadiabaticity, represented by the dashed line.

CSTIRAP. For the adiabatic passage, the system has to remain in a single dressed state throughout its evolution and the nonadiabatic effects should be negligible. Here we present a numerical analysis of nonadiabaticity and population transfer based on the dressed-state analysis in the field-interaction picture and show that a scheme can be engineered in such a way that nonadiabatic effects are suppressed through the proper choice of the detunings and the chirp rate.

The dressed-state energies of the four-level system are the roots of the quartic polynomial $f(\lambda(t))$ obtained using the Hamiltonian in Eq. (18). The effect of the two fields is to shift the quartic equation $f_0(\lambda(t))$ by a parabola $f_1(\lambda(t))$. The quartic polynomial $f(\lambda(t))$ reads

$$\begin{aligned} f(\lambda(t)) &= f_0(\lambda(t)) + f_1(\lambda(t)), \\ f_0(\lambda(t)) &= [\lambda(t) - 2\delta'(t)][\lambda(t) - 2\delta'(t) + 2\delta']\lambda(t) \\ &\quad \times [\lambda(t) - 2\Delta(t)], \\ f_1(\lambda(t)) &= 2|\Omega_{s_0}(t)|^2\{\lambda(t)[2\delta'(t) - \lambda(t)] - |\Omega_{p_0}(t)|^2[2\delta'(t) \\ &\quad - \lambda(t)][2\delta'(t) - 2\delta' - \lambda(t)]. \end{aligned} \quad (19)$$

This introduces mixing of the incoming dressed states having energies $\lambda_k^-(t)$ (where $t \rightarrow -\infty$) with the outgoing dressed states having energies $\lambda_k^+(t)$ (where $t \rightarrow +\infty$). The incoming and outgoing dressed states have energies given by the roots of $f_0(\lambda(t))$, which are obtained from the secular equation for the Hamiltonian (18) in the limit of vanishing field strength. The $f_1(\lambda(t))$ is the remainder polynomial in the general case of the nonzero external fields. The incoming and outgoing dressed-state energies are also the bare-state energies.

An understanding of the nonadiabatic contributions requires a study of dynamics in the vicinity of avoided crossings between the dressed-state energies, where $|\lambda_i(t) - \lambda_j(t)|/|\langle \lambda_i(t) | \dot{H}(t) | \lambda_j(t) \rangle| \leq 1$. The nontrivial coupling rate between two dressed states $|\lambda_i\rangle$ and $|\lambda_j\rangle$ is given by

$$\begin{aligned} V_{ij}(t) &= \left| \langle \lambda_i(t) | \frac{d}{dt} \lambda_j(t) \right| \\ &= \left| \frac{\langle \lambda_i(t) | \dot{H}(t) | \lambda_j(t) \rangle}{\lambda_i(t) - \lambda_j(t)} \right|, \quad i \neq j. \end{aligned} \quad (20)$$

The numerical dressed-state analysis of the selective population transfer in the four-level system is presented in Fig. 9, with Figs. 9(a)–9(d) corresponding to the case of the positive chirp rate shown in Fig. 7(b) and Figs. 9(e)–9(h) corresponding to the case of the negative chirp rate shown in Fig. 7(c). In Figs. 9(a) and 9(e) the bare-state energies $\lambda_k^\pm(t)$ (incoming and outgoing dressed energies) are represented by dashed lines and the dressed-state energies are represented by solid lines. A single dressed state $\lambda_k(t)$ does not connect to the same incoming and outgoing dressed states $\lambda_k^\pm(t)$. While the two $\lambda_k^\pm(t)$ are represented by a single dashed line, the time evolution of the k th dressed state $\lambda_k(t)$ results in its connection to the different outgoing $\lambda_m^+(t)$ state. At initial time $t \rightarrow -\infty$, the energy of eigenstate $|\lambda_1(t)\rangle$ starts at zero energy of the ground bare state $|1\rangle$. In the case of a positive chirp rate, the mechanism of selective population of the bare state $|4\rangle$ is through providing resonance via compensating the positive value of two-photon detuning by the choice of the positive chirp such that $\delta'(t) = -\delta' + \alpha(t_p - t_s) = 0$. This causes $\lambda_1(t) \approx 0$ for

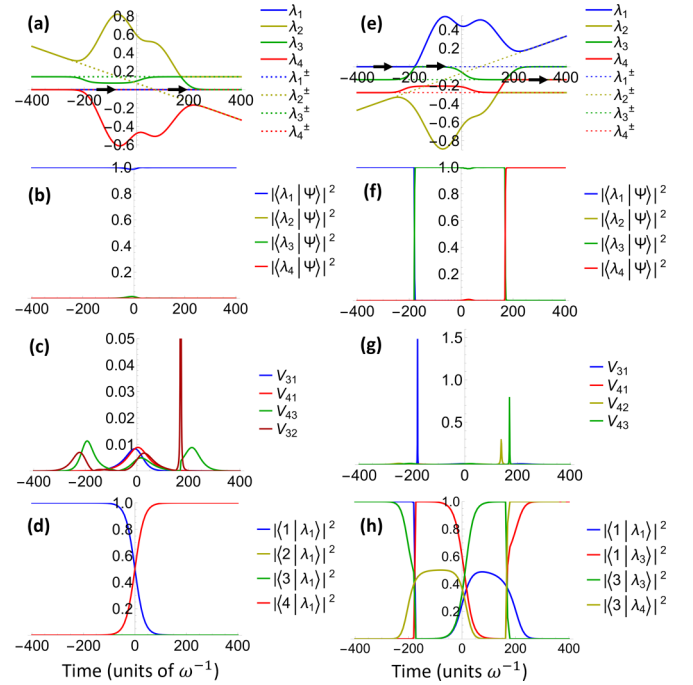


FIG. 9. Dressed-state analysis of the selective population transfer for cases with (a)–(d) a positive chirp rate, the dynamics for which is shown in Fig. 7(a), and (e)–(h) a negative chirp rate, corresponding to Fig. 7(b). The arrows in (a) and (e) represent the corresponding dressed state the system is aligned with during the evolution. The parameters are $\Delta = 0$, $t_s = -70\omega^{-1}$, $t_p = 70\omega^{-1}$, $\tau_{p,s} = 100\omega^{-1}$, and the peak Rabi frequencies $\Omega_{p,s_0} = 1.0\omega$. The chirp rate is $\alpha = \pm 1 \times 10^{-3}\omega^2$ for (a)–(d) and (e)–(h), respectively..

all time, as seen in Fig. 9(a), and results in a degeneracy for the bare states $\lambda_1^\pm(t) = \lambda_4^\pm(t)$. Owing to this, during the evolution, the system stays in a single dressed state $|\lambda_1(t)\rangle$, which evolves from bare state $|1\rangle$ to $|4\rangle$ [Fig. 9(d)]. The solid arrows along $\lambda_1(t)$ indicate that the system is in the respective dressed state $|\lambda_1(t)\rangle$ all the time. The dressed state $|\lambda_1(t)\rangle$ is the dark state. The probability amplitudes of the dressed states with respect to the state vector $|\psi(t)\rangle$, shown in Fig. 9(b), confirm the adiabatic evolution of the wave function along the dressed state $|\lambda_1(t)\rangle$, since it is isolated from the rest manifold. The nonadiabatic coupling terms, shown in Fig. 9(c), with the exception of the coupling between $|\lambda_2(t)\rangle$ and $|\lambda_3(t)\rangle$, are an order of magnitude less than the closest separation of the dressed states, which confirms the adiabatic passage as a mechanism of population transfer. The high value of the coupling rate $\langle \lambda_3(t) | \frac{d}{dt} \lambda_2(t) \rangle$, which coincides with the avoided crossing between the corresponding eigenenergies at $t \approx 200\omega^{-1}$, does not adversely affect the adiabaticity as the total wave function aligns with $|\lambda_1(t)\rangle$ at all times.

In contrast to the previous case, the time evolution of dressed states for a negative value of the chirp, shown in Figs. 9(e)–9(h), demonstrates a complete population transfer from $|1\rangle$ to the resonant state $|3\rangle$ via a nonadiabatic process involving three dressed states. Two nonadiabatic transitions occur at a low-field intensity while a smooth (adiabatic-type) population transfer takes place within a single dressed state at strong fields. In more detail, at time $t \approx -200\omega^{-1}$, the

originally populated dressed state $|\lambda_1(t)\rangle$, keeping population within the bare state $|1\rangle$, approaches an avoided crossing with $|\lambda_3(t)\rangle$, shown in Fig. 9(e), and transfers population there owing to nonzero coupling shown in Fig. 9(g). Further time evolution takes place within $|\lambda_3(t)\rangle$, during which bare states $|1\rangle$ and $|3\rangle$ adiabatically exchange population. At time $t \approx 200\omega^{-1}$, the second avoided crossing of $|\lambda_3(t)\rangle$ occurs with dressed state $|\lambda_4(t)\rangle$. Here the population is transferred again populating bare state $|3\rangle$ within $|\lambda_4(t)\rangle$ by the end of the pulses' duration, as shown in Fig. 9(h). The nonadiabatic couplings, shown in Fig. 9(g), at the same times as the avoided crossings, provide population transfer between respective dressed states. The slopes of the dressed-state energy curves and the closest-approach distance between the curves at the crossing give us an estimate of the transition probability. The closest-approach distance is $8 \times 10^{-4}\omega$ at $t_a = 198.1\omega^{-1}$, $|\frac{d}{dt}[\lambda_3(t_a) - \lambda_4(t_a)]| = 3.48 \times 10^{-4}\omega$, and the nonadiabatic coupling $\langle \lambda_4(t) | \frac{d}{dt} \lambda_3(t) \rangle$ is a Lorentzian curve centered at $t = t_a$ with width $w = 0.35$ and area $A = \pi/2$. The population is transferred from bare state $|1\rangle$ to bare state $|3\rangle$ nonadiabatically, owing to the synergistic dynamics between dressed states shown in Fig. 9(f), first $|\lambda_1(t)\rangle$ and $|\lambda_3(t)\rangle$ and then $|\lambda_3(t)\rangle$ and $|\lambda_4(t)\rangle$. Notably, the majority of population transfer occurs during the time the two pulses overlap.

As demonstrated in Fig. 9, the population transfer to the resonant state $|3\rangle$ is not an adiabatic process. However, it is possible to transfer the population to $|3\rangle$ via adiabatic passage by introducing a chirping delay in the Stokes pulse. The modified Stokes pulse with delay t_d reads

$$E_s(t) = E_{s_0} e^{-(t-t_s)^2/\tau_s^2} \cos \left[\omega_s(t - t_s) + \frac{1}{2}\beta(t - t_s - t_d)^2 \right]. \quad (21)$$

This modifies the $\delta'(t)$ in Eq. (18) to $\delta'(t) = -\delta' + \beta(t - t_s - t_d) - \alpha(t - t_p)$. With a choice of $t_d = t_p - t_s$, the third diagonal element cancels out, making the states $|1\rangle$ and $|3\rangle$ degenerate. This is the condition to populate $|3\rangle$ adiabatically. The evolution of dressed-state energies in this case is given in Fig. 10(a). Here the dark state $|\lambda_3(t)\rangle$, which the system is always aligned with, as seen in Fig. 10(b), smoothly evolves from bare state $|1\rangle$ to bare state $|3\rangle$, shown in Fig. 10(d). All the nonadiabatic coupling rates are negligible compared to the dressed-state energy separations, confirming the passage is adiabatic. In Fig. 11 a contour plot of population ρ_{33} is depicted as a function of the two-photon detuning δ' and the chirp rate α . The figure demonstrates that, for adiabatic population transfer to state $|3\rangle$, there is no constraint condition on the value of the chirp rate within the given range as long as a delay t_d is applied and satisfies the above condition.

The selectivity of the final-state excitation is possible only for small values of chirp rates satisfying the Landau-Zener adiabaticity condition requiring $\Omega_{p_0, s_0}^2/\alpha \gg 1$. For larger values of chirp rates, adiabatic passage is not possible, leading to an arbitrary superposition of states $|3\rangle$ and $|4\rangle$.

IV. CFSTIRAP

A. CFSTIRAP in the three-level λ system

As demonstrated in Sec. II, the two-photon resonance is required for the maximum coherence in FSTIRAP. Here we

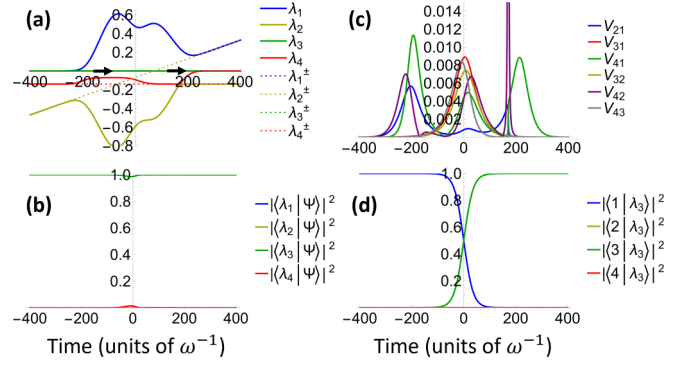


FIG. 10. Adiabatic population transfer to the resonant state $|3\rangle$ by applying a chirping delay $t_d = t_p - t_s$ in the Stokes pulse. (a) Evolution of dressed-state energies. (b) The wave function $|\psi(t)\rangle$ is always aligned with the dressed state $|\lambda_3(t)\rangle$, which smoothly evolves from bare state $|1\rangle$ to $|3\rangle$. (c) There is an avoided crossing between states $|2\rangle$ and $|4\rangle$, implying a high value of $V_{42} = \langle \lambda_4(t) | \frac{d}{dt} \lambda_2(t) \rangle$. The coupling does not include the dark state $|3\rangle$, confirming that the process is adiabatic.

introduce the chirped FSTIRAP (CFSTIRAP) as the means to maximize coherence when the two-photon detuning is nonzero. Consider the pump in which the first and the second Stokes pulse components are chirped with chirp rates α , β_1 , and β_2 , respectively,

$$E_p(t) = E_{p_0} \sin A e^{-(t-t_p)^2/\tau^2} \cos \left[\omega_p(t - t_p) + \frac{1}{2}\alpha(t - t_p)^2 \right],$$

$$E_s(t) = E_{s_0} e^{-(t+t_p)^2/\tau^2} \cos \left[\omega_s(t + t_p) + \frac{\beta_1}{2}(t + t_p - t_{d1})^2 \right] + E_{s_0} \cos A e^{-(t-t_p)^2/\tau^2} \times \cos \left[\omega_s(t - t_p) + \frac{\beta_2}{2}(t - t_p - t_{d2})^2 \right], \quad (22)$$

where the chirping of the first and the second Stokes pulses is assumed to have delays t_{d1} and t_{d2} , respectively. To derive the field-interaction Hamiltonian, the following transformations

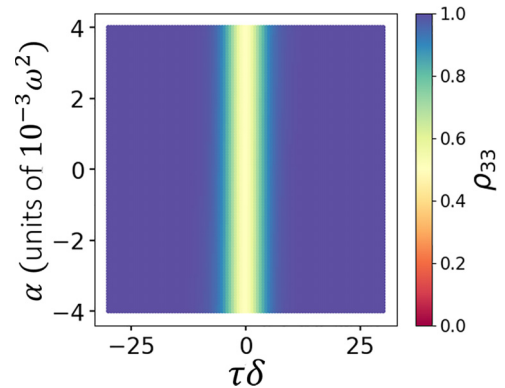


FIG. 11. Population of resonant state $|3\rangle$ as a function of $\tau\delta'$ and chirp rate α for the case when a chirping delay $t_d = t_p - t_s$ is applied in the Stokes pulse. A full population transfer to the state $|3\rangle$ occurs adiabatically for all chirp values in this range owing to the degeneracy between states $|1\rangle$ and $|3\rangle$.

are applied:

$$\begin{aligned} a_1(t) &= \tilde{a}_1(t)e^{i\omega_p(t-t_p)}, \\ a_2(t) &= \tilde{a}_2(t)e^{-i(\alpha/2)(t-t_p)^2}, \\ a_3(t) &= \tilde{a}_3(t)e^{i\omega_s(t+t_p)+i(\beta_1/2)(t+t_p-t_{d1})^2-i(\alpha/2)(t-t_p)^2}. \end{aligned} \quad (23)$$

Then the Hamiltonian describing CFSTIRAP in the field-interaction representation reads

$$\mathbf{H}(t) = \frac{\hbar}{2} \times \begin{pmatrix} 0 & \Omega_{p0}(t) & 0 \\ \Omega_{p0}(t) & 2\Delta(t) & \Omega_{s10}(t) + \Omega_{s20}(t)e^{i\eta(t)} \\ 0 & \Omega_{s10}(t) + \Omega_{s20}(t)e^{-i\eta(t)} & 2\delta(t) \end{pmatrix}, \quad (24)$$

where the Rabi frequencies are the same as in Eq. (7), the time-dependent detuning is $\delta(t) = -\delta + \beta_1(t + t_p - t_{d1}) - \alpha(t - t_p)$, and the time-dependent phase $\eta(t)$ is

$$\eta(t) = 2\omega_s t_p + \frac{\beta_1}{2}(t + t_p - t_{d1})^2 - \frac{\beta_2}{2}(t - t_p - t_{d2})^2. \quad (25)$$

If all the chirp rates are equal $\alpha = \beta_1 = \beta_2$ and the chirping delay t_{d1} is chosen to be $t_{d1} = 0$, then the time-dependent detuning $\delta(t)$ becomes $\delta(t) = -\delta + 2\alpha t_p$. In addition, if the delay t_{d2} is given by the negative time difference between the peaks of two Stokes pulses, $t_{d2} = -2t_p$, then the phase $\eta(t)$ becomes a constant independent from the chirp rates, $\eta(t) = 2\omega_s t_p = \zeta$. These assumptions result in the real values of the Rabi frequencies and the straightforward condition for the resonance with state $|3\rangle$, $\alpha = \delta/2t_p$.

The Hamiltonian in Eq. (24) is diagonalized using the $\mathbf{T}(t)$ matrix in Eq. (11) with the new Stokes field $\tilde{\Omega}_{s0}(t) = \Omega_{s10}(t) + \Omega_{s20}(t)e^{-i\zeta}$ after imposing the condition that $\delta(t) = 0$. In Fig. 12 the dressed-state energies, populations, and coherence dynamics are plotted as a function of time for $\delta < 0$ and $\delta > 0$. The population dynamics shows that it is possible to create the maximum coherence in the absence of the two-photon resonance by carefully choosing the chirp rates and chirping delay, satisfying the condition $\delta(t) = 0$. The system is always aligned with the dark state $|\lambda_0(t)\rangle$, which is again given by Eq. (17), with the modified mixing angle $\theta(t) = \Omega_{p0}(t)/|\tilde{\Omega}_{s0}(t)|$. Owing to the modified Stokes field, as $t \rightarrow \infty$, $\theta(t) = \tan^{-1}(1) = \pi/4$ and the dark state now evolves from state $|\tilde{1}\rangle$ to $1/\sqrt{2}(|\tilde{1}\rangle - |\tilde{3}\rangle)$, which is a maximally coherent superposition between the two states. The tilde will again be dropped for convenience for the remainder of this section.

The contour plot of coherence between the initial and the final states, ρ_{13} , as a function of the two-photon detuning δ and the chirp rate α is shown in Fig. 13. The maximum coherence window, shown in blue, is achieved and remains relatively constant for the chirp values $\alpha = \delta/2t_p$ satisfying the condition $\delta(t) = 0$. This is in stark contrast to Fig. 3(b), in which state coherence decreased with the increase of the two-photon detuning. Thus, the delayed chirp in the CFSTIRAP configuration overcomes the problem of maximizing state coherence adiabatically in the presence of the two-photon detuning.

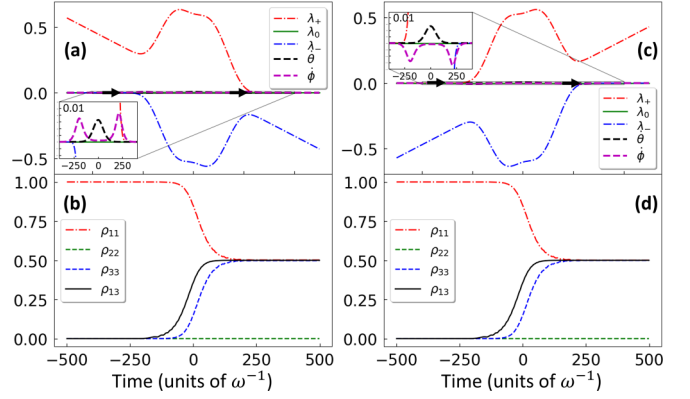


FIG. 12. Evolution of the dressed states, the nonadiabatic parameter V_{ij} , and the state coherence in the case of CFSTIRAP for detuning (a) and (b) $\delta > 0$ and (c) and (d) $\delta < 0$. A maximum coherence is created in both cases because of the choice of chip rates satisfying $\delta(t) = 0$. The value of V_{ij} remains zero except for a short duration, as shown in the inset. The system remains in the dark state $|\lambda_0\rangle$ throughout the evolution, as indicated by the arrows. In (a) and (b) $\delta = -0.14\omega$ and $\alpha = -1 \times 10^{-3}\omega^2$ and in (c) and (d) $\delta = 0.14\omega$ and $\alpha = 1 \times 10^{-3}\omega^2$. The other parameters are $\Delta = 0$, $\tau_{p,s} = 100\omega^{-1}$, and peak $\Omega_{p0,s0} = 1.0\omega$.

B. CFSTIRAP in a four-level λ system with two energetically close final states

In Sec. III C it was shown that, using the CSTIRAP scheme, the population can be driven completely to a desired final state in a nearly degenerate four-level λ system (Fig. 6). Motivated by this result, we show that, using CFSTIRAP, it is possible to create a system with equal populations distributed between the initial state and one of the final states in the four-level system. In this case, the chirping of one of the Stokes pulses needs to be delayed for the selective final-state excitation. The respective Hamiltonian in the field-interaction frame for the four-level system is written by extending the three-level Hamiltonian in Eq. (24) to a four-level

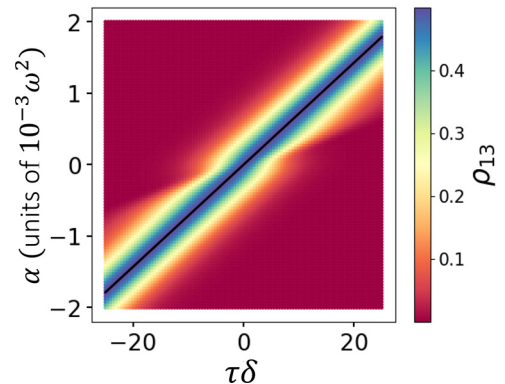


FIG. 13. Coherence in CFSTIRAP as a function of two-photon detuning and chirp rate. The adiabatic regime and maximum coherence are achieved in the vicinity of the dark line satisfying $\alpha = \delta/2t_p$, corresponding to $\delta(t) = 0$.

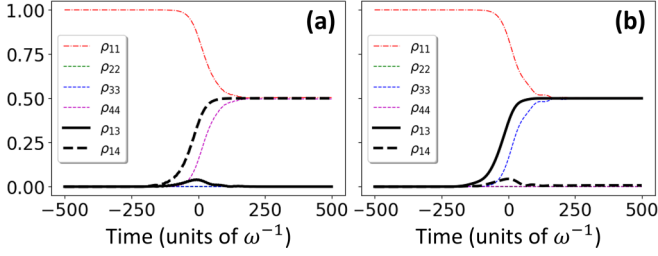


FIG. 14. Evolution of populations and coherence in the case of CFSTIRAP for $\delta' = 0.14\omega$. (a) When the chirping delays are chosen to be $t_{d1} = 0$ and $t_{d2} = -2t_p$, the coherence ρ_{14} is maximized without populating state $|3\rangle$. (b) In contrast, when $t_{d1} = 2t_p$ and $t_{d2} = 0$ the states $|1\rangle$ and $|3\rangle$ have equal populations and coherence ρ_{13} is maximized without populating state $|4\rangle$.

system as

$$\mathbf{H}(t) = \frac{\hbar}{2} \times \begin{pmatrix} 0 & \Omega_{p0}(t) & 0 & 0 \\ \Omega_{p0}(t) 2[\Delta - \alpha(t - t_p)] & \tilde{\Omega}_{s0}^*(t) & \tilde{\Omega}_{s0}^*(t) & \\ 0 & \tilde{\Omega}_{s0}(t) & 2[\delta'(t) + \delta'] & 0 \\ 0 & \tilde{\Omega}_{s0}(t) & 0 & 2\delta'(t) \end{pmatrix}, \quad (26)$$

where

$$\begin{aligned} \tilde{\Omega}_{s0}(t) &= \Omega_{s10}(t) + \Omega_{s20}(t)e^{-i\eta(t)}, \\ \delta'(t) &= -\delta' + \beta_1(t + t_p - t_{d1}) - \alpha(t - t_p), \\ \eta(t) &= 2\omega_s t_p + \frac{\beta_1}{2}(t + t_p - t_{d1})^2 - \frac{\beta_2}{2}(t - t_p - t_{d2})^2. \end{aligned}$$

If the chirp rates are chosen to be $\alpha = \beta_1 = \beta_2 = \delta'/2t_p$, the fourth diagonal term becomes zero and the phase $\eta(t)$ becomes a constant $\eta(t) = 2\omega_s t_p = \zeta$ for the choice of chirping delays to be $t_{d1} = 0$ and $t_{d2} = -2t_p$. This results in the creation of the maximum coherence between states $|1\rangle$ and $|4\rangle$, without populating any other states. The evolution of populations and coherence in this case is shown in Fig. 14(a). In a contrary scenario, a maximally coherent superposition is obtained between the initial and final resonant states $|3\rangle$ when the chirp rates are chosen to be $\alpha = \beta_1 = \beta_2 = \delta'/2t_p$ and chirping delays $t_{d1} = 2t_p$ and $t_{d2} = 0$. In this case, the third diagonal term becomes zero and the phase is again reduced to the same constant $\eta(t) = 2\omega_s t_p = \zeta$. The evolution of the state populations and coherence in this case is shown in Fig. 14(b).

The robustness of the schemes corresponding to Figs. 14(a) and 14(b) are shown in Figs. 15(a) and 15(b) respectively. In Fig. 15(a), the coherence ρ_{14} is maximized in the vicinity of the straight line satisfying $\alpha = \delta'/2t_p$. Contrary to this, there are no constraint conditions on the chirp rate to maximize the coherence ρ_{13} , as shown in Fig. 15(b).

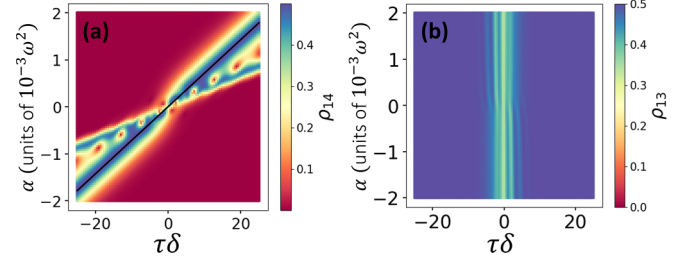


FIG. 15. (a) Coherence ρ_{14} as a function of two-photon detuning and chirp rate α for a choice of chirping delays $t_{d1} = 0$ and $t_{d2} = -2t_p$ and (b) ρ_{13} for $t_{d1} = 2t_p$ and $t_{d2} = 0$. In (a) a maximum coherence between the initial and detuned state $|4\rangle$ is reached for chirp rates satisfying $\alpha = \delta'/2t_p$, represented by the diagonal dark line. As demonstrated in (b), there is no constraint condition on the chirp rate to create a maximally coherent superposition between the initial and resonant state $|3\rangle$ as long as the delays satisfy $t_{d1} = t_p$ and $t_{d2} = 0$.

C. Dressed-state analysis of CFSTIRAP in the four-level λ system

In FSTIRAP, the choice of the fields in Eq. (7) gives us a different structure in the dressed-state picture as compared to STIRAP. In the three-level system, the dressed states are nondegenerate at $t \rightarrow -\infty$ but the states $|\lambda_1\rangle$ and $|\lambda_3\rangle$ are degenerate at $t \rightarrow \infty$.

The Schrödinger equation in the dressed-state basis is $\dot{\Psi}(t) = -i[E(t) + F(t)]\Psi(t)$, where $E_{ij}(t) = [\lambda_i(t) + \langle v_i(t) | \dot{v}_i(t) \rangle \delta_{ij}]$ represents the diagonal adiabatic matrix and $F_{ij}(t) = \langle v_i(t) | \dot{v}_j(t) \rangle (1 - \delta_{ij})$ represents the nonadiabatic coupling matrix. The nonadiabatic transitions need to be removed to achieve adiabatic passage, and this requires choosing parameters that prevent any avoided crossings and transitions between dressed states.

The time of avoided crossings between two dressed states can be found when the determinant of $H(t)$ and its derivative are both zero. There is also the possibility of a crossing with three or more dressed states. The probability of transitioning to the higher-energy state $|\lambda_j(t)\rangle$, assuming all population is initially in state $|\lambda_i(t)\rangle$, during an avoided crossing at time t where $\lambda_i(t) = \lambda_j(t)$, is given by the Landau-Zener formula [23]

$$P_{LZ}(t) = \exp\left(-\frac{4\pi^2}{\hbar} \frac{[\langle \lambda_j(t) | \frac{d}{dt} \lambda_i(t) \rangle]^2}{\frac{d}{dt} |\lambda_i(t) - \lambda_j(t)|}\right). \quad (27)$$

We note that while there can be many avoided crossings when the Rabi frequencies are small, these crossings trivially affect the bare-state populations. The above discussions about the dressed-state analysis are generic and are not specific to the case of CFSTIRAP.

The energy gap between the two dressed states at $t \rightarrow \infty$, assuming we have no other nonadiabatic transitions, will determine the final state. The previous section gives us a scheme for which we can achieve adiabatic evolution to a maximum-coherence state composed of equal population in the ground state and one of the final states $|3\rangle$ or $|4\rangle$. The selection of the latter state depends on the chirp rate and frequency offsets, created by the delays t_{d1} and t_{d2} introduced in the

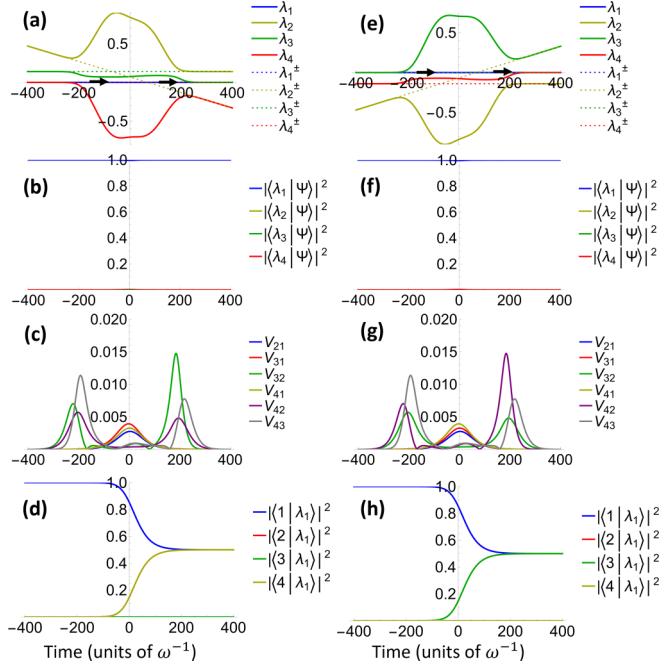


FIG. 16. Dressed-state analysis of the CFSTIRAP four-level system, corresponding to (a)–(d) Fig. 14(a) when ρ_{14} is maximized and (e)–(h) Fig. 14(b) when ρ_{13} is maximized. (a) and (e) The system is always aligned with the dressed state $|\lambda_1\rangle$, as indicated by the arrows. (b) and (f) Dressed-state decomposition of the wave function confirms adiabatic evolution, with (c) and (g) trivial nonadiabatic coupling rates. The dressed state $|\lambda_1\rangle$ smoothly evolves to a maximum coherence state involving (d) $|1\rangle$ and $|4\rangle$ and (h) $|1\rangle$ and $|3\rangle$. The parameters are $\Delta = 0$, $t_s = -70\omega^{-1}$, $t_p = 70\omega^{-1}$, $\tau_{p,s} = 100\omega^{-1}$, $\Omega_{p_0,s_0} = 1.0\omega$, and $\alpha = \pm 1 \times 10^{-3}\omega^2$.

chirp functions. For adiabatic evolution, the energy spectrum of the Hamiltonian that satisfies this condition must be the one where the ground state and the selected state coincide at the same energy at $t \rightarrow \infty$ and the nonselected state must diverge from the two previous states. This condition is required for the system to remain in a single dressed state.

The analysis of the evolution of the dressed-state energies, shown in Fig. 16, confirms that the creation of the maximum coherence in the four-level system via selective excitation in Fig. 14 is perfectly adiabatic. Figures 16(a)–16(d) correspond to Fig. 14(b), where the delays are chosen to be $t_{d1} = 0$ and $t_{d2} = -2t_p$, and Figs. 16(e)–16(h) correspond to Fig. 14(c), where $t_{d1} = 2t_p$ and $t_{d2} = 0$. The system remains in the dressed (dark) state throughout the process, which smoothly evolves to a maximum superposition between $|1\rangle$ and $|4\rangle$ in Fig. 16(d) and between $|1\rangle$ and $|3\rangle$ in Fig. 16(h). The behavior of dressed states in Figs. 16(f)–16(h) is the same as in Figs. 16(b)–16(d), respectively, except that $|\lambda_3\rangle$ takes up the role of $|\lambda_4\rangle$ and vice versa. The rates of nonadiabatic couplings in Figs. 16(b) and 16(f) also confirm that the evolution is adiabatic as all of them have magnitudes much less than the difference between dressed energies.

V. CSTIRAP AND CFSTIRAP IN THE NV CENTER IN DIAMOND

In this section we consider population transfer in the ground state of the ^{15}N -vacancy center in diamond to illus-

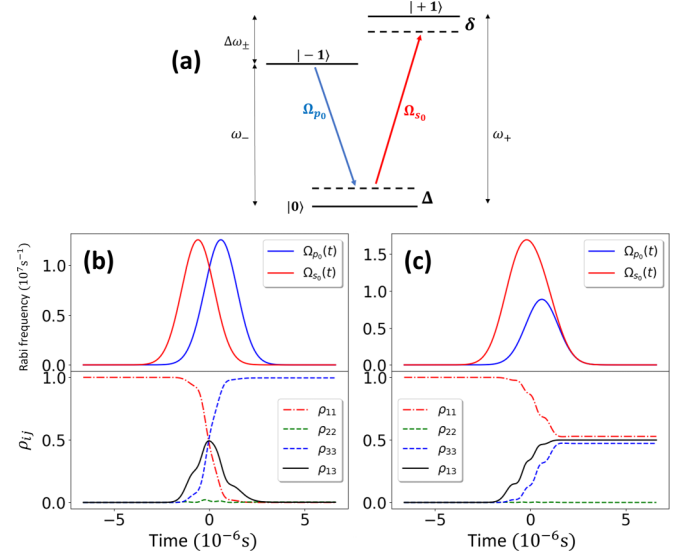


FIG. 17. CSTIRAP and CFSTIRAP in the ground state of the NV center in diamond. (a) Electron spin energy levels where the degeneracy between $|\pm 1\rangle$ states is lifted by an external magnetic field. (b) Population transfer from $|-1\rangle$ to $|+1\rangle$ using the CSTIRAP scheme. (c) Applying the CFSTIRAP scheme, we create a maximally coherent superposition between states $|-1\rangle$ and $|+1\rangle$.

trate the implementation of the CSTIRAP and CFSTIRAP schemes. The electron spin states of the NV center in diamond [the energy structure shown in Fig. 17(a)] have been extensively investigated, in particular implementing STIRAP [3]. In the absence of an external magnetic field, the states $|\pm 1\rangle$ are degenerate, having an energy difference of 2.87 GHz with state $|0\rangle$. The degeneracy is lifted by applying a magnetic field B_z along the z axis, resulting in the energy split of $\Delta\omega_{\pm} = 2\gamma_e B_z$, where γ_e is the electronic gyromagnetic ratio given by $\gamma_e = 28.0 \text{ GHz T}^{-1}$. For $B_z = 3.81 \times 10^{-2} \text{ T}$, this split becomes $\Delta\omega_{\pm} = 2.13 \text{ GHz}$. Two Raman microwave pulses, in resonance with the transition frequencies ω_- and ω_+ , are used to transfer the population from $|-1\rangle$ to $|+1\rangle$. An efficient STIRAP population transfer using Gaussian pulses with the peak Rabi frequencies $\Omega_{p_0,s_0} = 4\pi \times 10^6 \text{ s}^{-1}$, the pulse durations $\tau_{p,s} = 0.85\sqrt{2} \mu\text{s}$, and the time delay $t_p - t_s = 1.2 \mu\text{s}$ has been demonstrated in [3]. Note that it was done under the one-photon and two-photon resonance conditions.

When the two-photon resonance condition cannot be satisfied, pulses with equal chirp rates can be used to compensate for the two-photon detuning, as demonstrated above. For example, for $\delta = 0.1\Delta\omega_{\pm} \approx 0.2 \text{ GHz}$ and time delay $t_p - t_s = 1.2 \mu\text{s}$, the chirp rate needs to be $\alpha = \delta/(t_p - t_s) = \delta/2t_p = 0.17 \text{ GHz}/\mu\text{s}$ in both CSTIRAP [Fig. 17(b)] and CFSTIRAP [Fig. 17(c)]. In the case of CFSTIRAP, additionally, the chirping of the second Stokes pulse component needs to be ahead of its frequency by $2t_p = 1.2 \mu\text{s}$ to ensure the cancellation of the phase between the two Stokes pulse components. When these conditions are met, the evolution of populations and coherence in both CSTIRAP and CFSTIRAP is almost identical to the resonant cases as in [3]. These results demonstrate the validity of the proposed methodology to perform adiabatic

passage within a single dressed state, the dark state, in the presence of the two-photon detuning.

VI. SUMMARY

We presented a scheme that selectively creates the maximum coherence in a four-level system having two nearly degenerate final states via CFSTIRAP. First, by analyzing the dressed-state dynamics, we demonstrated that chirping of the pump and the Stokes pulses in STIRAP allows one to achieve adiabaticity in the absence of the two-photon resonance. To eliminate the nonadiabatic contribution, both pulses must be chirped at the same rate and the value of two-photon detuning δ must match the product of chirp rate and the time delay between the pulses $\alpha(t_p - t_s)$. If the resonance frequency is unknown, this protocol may be used to determine the energy levels by tuning the chirp rate to compensate for the detuning. We then analyzed a four-level system with two nearly degenerate terminal levels and showed that the population can be driven exclusively to one of the terminal levels by the appropriate pulse chirping. For negative two-photon detuning, the detuned final state is populated if the chirp rate is positive while the resonant state is populated if the rate is negative. The constraint conditions on the chirp rate in both cases were discussed. The analysis of the evolution of the dressed states revealed that the population transfer to the detuned state is adiabatic while the population transfer to the resonant state is nonadiabatic. Further, we showed that the population can be adiabatically driven to the resonant state by introducing a delay in the chirping of the Stokes pulse. We applied the concept of the delay in the chirping to FSTIRAP and showed that, by chirping the pump and Stokes pulses equally and introducing a chirping delay in the second Stokes pulse component, the adiabatic creation of the maximally coherent superposition is possible even in the absence of the two-photon resonance. We applied the CFSTIRAP technique to the four-level system and demonstrated that the maximal coherence between the initial and a predetermined final state is achievable by manipulating the chirping delays of Stokes pulse components. The

analysis of the evolution of the dressed states confirms that the selective excitation in the four-level system is perfectly adiabatic owing to the choice of the chirp rates and the chirp delays.

For practical implementations, we note that there is an upper limit on the value of two-photon detuning that can be compensated by the choice of the chirp rate in both the three-level and the four-level systems. This is due to the limits on the values of possible temporal chirp rates for a given pulse duration and the requirement to have a significant overlap between the pulses for adiabatic passage. For a given pulse duration τ , the optimal time difference between the pump and the Stokes pulses is $t_p - t_s = 1.4\tau$. For $\tau = 100\omega^{-1}$, the possible values of the chirp rates are $\alpha \approx \pm 1 \times 10^{-5}\omega^2$, implying the upper limit on the two-photon detuning $|\delta| \lesssim |\alpha|(t_p - t_s) = 0.007\omega$. In the three-level system, the detuning should not exceed this value to satisfy the adiabaticity condition and in the four-level system, a superposition of the initial and a predetermined final state detuned up to this value may be generated, while the final-state selectivity is limited by $|\alpha(t_p - t_s)|$.

Maximizing coherence is critical to optimizing the output signal in imaging and sensing techniques based on coherent Raman spectroscopy. Due to its adiabaticity, reliability, and higher spectral resolution, the method presented here will find application in various areas of quantum science and technology, such as quantum information, quantum sensing, and imaging, metrology, and magnetometry.

ACKNOWLEDGMENTS

S.A.M., J.C., and A.R. acknowledge support from the Office of Naval Research under Awards No. N00014-20-1-2086 and No. N00014-22-1-2374. S.A.M. acknowledges the Helmholtz Institute Mainz Visitor Program and the Alexander von Humboldt Foundation. J.C. was also partially supported by DEVCOM Army Research Laboratory under Cooperative Agreement No. W911NF2320076. D.B. was partially supported by DEVCOM Army Research Laboratory under Cooperative Agreement N. W911NF2120180.

-
- [1] U. Gaubatz, P. Rudecki, S. Schiemann, and K. Bergmann, Population transfer between molecular vibrational levels by stimulated Raman scattering with partially overlapping laser fields, A new concept and experimental results, *J. Chem. Phys.* **92**, 5363 (1990).
 - [2] K. Bergmann *et al.*, Roadmap on STIRAP applications, *J. Phys. B* **52**, 202001 (2019).
 - [3] F. Böhm, N. Nikolay, S. Neinert, C. E. Nebel, and O. Benson, Ground-state microwave-stimulated Raman transitions and adiabatic spin transfer in the ^{15}N nitrogen vacancy center, *Phys. Rev. B* **104**, 035201 (2021).
 - [4] C. Weinzettl, J. Görlitz, J. N. Becker, I. A. Walmsley, E. Poem, J. Nunn, and C. Becher, Coherent control and wave mixing in an ensemble of silicon-vacancy centers in diamond, *Phys. Rev. Lett.* **122**, 063601 (2019).
 - [5] R. Bause, A. Kamijo, X.-Y. Chen, M. Duda, A. Schindewolf, I. Bloch, and X.-Y. Luo, Efficient conversion of closed-channel-dominated Feshbach molecules of $^{23}\text{Na}^{40}\text{K}$ to their absolute ground state, *Phys. Rev. A* **104**, 043321 (2021).
 - [6] F. Setiawan, P. Groszkowski, and A. A. Clerk, Fast and robust geometric two-qubit gates for superconducting qubits and beyond, *Phys. Rev. Appl.* **19**, 034071 (2023).
 - [7] D. Guéry-Odelin, A. Ruschhaupt, A. Kiely, E. Torrontegui, S. Martínez-Garaot, and J. G. Muga, Shortcuts to adiabaticity: Concepts, methods, and applications, *Rev. Mod. Phys.* **91**, 045001 (2019).
 - [8] T. Kirschbaum, N. Minkov, and A. Pálffy, Nuclear coherent population transfer to the $^{229\text{m}}\text{Th}$ isomer using x-ray pulses, *Phys. Rev. C* **105**, 064313 (2022).

- [9] G. T. Genov, S. Rochester, M. Auzinsh, F. Jelezko, and D. Budker, Robust two-state swap by stimulated Raman adiabatic passage, *J. Phys. B* **56**, 054001 (2023).
- [10] I. R. Sola, B. Y. Chang, S. A. Malinovskaya, S. C. Carrasco, and V. S. Malinovsky, Stimulated Raman adiabatic passage with trains of weak pulses, *J. Phys. B* **55**, 234002 (2022).
- [11] Z. Huang, G. K. Brennen, and Y. Ouyang, Imaging stars with quantum error correction, *Phys. Rev. Lett.* **129**, 210502 (2022).
- [12] N. V. Vitanov, K.-A. Suominen, and B. W. Shore, Creation of coherent atomic superpositions by fractional stimulated Raman adiabatic passage, *J. Phys. B* **32**, 4535 (1999).
- [13] V. A. Sautenkov, C. Y. Ye, Y. V. Rostovtsev, G. R. Welch, and M. O. Scully, Enhancement of field generation via maximal atomic coherence prepared by fast adiabatic passage in Rb vapor, *Phys. Rev. A* **70**, 033406 (2004).
- [14] S. A. Malinovskaya, Chirped pulse control methods for imaging of biological structure and dynamics, *Int. J. Quantum Chem.* **107**, 3151 (2007).
- [15] S. M. Rochester, K. Szymański, M. Raizen, S. Pustelny, M. Auzinsh, and D. Budker, Efficient polarization of high-angular-momentum systems, *Phys. Rev. A* **94**, 043416 (2016).
- [16] N. Pandya, G. Lui, F. A. Narducci, J. Chathanathil, and S. A. Malinovskaya, Creation of the maximum coherence via adiabatic passage in the four-wave mixing process of coherent anti-Stokes Raman scattering, *Chem. Phys. Lett.* **738**, 136763 (2020).
- [17] J. Chathanathil, G. Liu, and S. A. Malinovskaya, Semiclassical control theory of coherent anti-Stokes Raman scattering maximizing vibrational coherence for remote detection, *Phys. Rev. A* **104**, 043701 (2021).
- [18] Y. B. Band and O. Magnes, Chirped adiabatic passage with temporally delayed pulses, *Phys. Rev. A* **50**, 584 (1994).
- [19] J. S. Melinger, S. R. Gandhi, A. Hariharan, J. X. Tull, and W. S. Warren, Generation of narrowband inversion with broadband laser pulses, *Phys. Rev. Lett.* **68**, 2000 (1992).
- [20] J. S. Melinger, S. R. Gandhi, A. Hariharan, D. Goswami, and W. S. Warren, Adiabatic population transfer with frequency-swept laser pulses, *J. Chem. Phys.* **101**, 6439 (1994).
- [21] N. V. Vitanov, A. A. Rangelov, B. W. Shore, and K. Bergmann, Stimulated Raman adiabatic passage in physics, chemistry, and beyond, *Rev. Mod. Phys.* **89**, 015006 (2017).
- [22] I. I. Boradjev and N. V. Vitanov, Stimulated Raman adiabatic passage with unequal couplings: Beyond two-photon resonance, *Phys. Rev. A* **81**, 053415 (2010).
- [23] M. V. Danileiko, V. I. Romanenko, and L. P. Yatsenko, Landau-Zener transitions and population transfer in a three-level system driven by two delayed laser pulses, *Opt. Commun.* **109**, 462 (1994).